Supplementary Information (SI) for ChemComm.
This journal is © The Royal Society of Chemistry 2026

Imaging the Reactivity of Carbon Nitride Nanosheets by Photoinduced Cathodic Electrochemiluminescence Microscopy

Chuan Li,[a,b] *Wei Zhang,*[a,b*] *Changlin Zhou,*[b] *Fatima Merhi,*[b] *Bertrand Goudeau,*[b] *Patrick Garrigue,*[b] *Gabriel Loget* [b]* *and Neso Sojic,*[b]*

[a] School of Chemistry and Chemical Engineering, Liaocheng University, Liaocheng, Shandong, 252059, China

[b] Univ. Bordeaux, Bordeaux INP, ISM, UMR 5255 CNRS, Site ENSMAC, 33607 Pessac, France.

Author Information

Corresponding authors

*E-mail: weizhanglc@163.com

*E-mail: gabriel.loget@cnrs.fr

*E-mail: sojic@u-bordeaux.fr

1 Experimental section

1.1 Chemicals. Dicyandiamide (DCDA, 99%) was purchased from Sigma-Aldrich. Acetone (VLSI electronic grade, from VWR Chemicals) and ethanol absolute (VLSI electronic grade, from Avantor Science) were used without further purification. Ultrapure Water (18.2 MΩ cm) was used and sterilized throughout the experiments.

1.2 The preparation of CNNS

The bulk CN samples were prepared according to the previously reported literatures[1]. For bulk CN, 10 g of DCDA was placed in a capped crucible and heated at 550 ℃ in air for 4 h with a 4 h ramp time in a muffle furnace. The CNNS were prepared by ultrasonic exfoliation, respectively. Briefly, 10 mg of obtained bulk sample was dispersed in 10 mL of ethanol absolute, and ultrasonicated for about 18 h. The initial formed suspension was then centrifuged at 7000 rpm for 20 min to remove the residual un-exfoliated nanoparticle and large area nanosheets for PECL experiments.

Because of their low ECL efficiency and poor dispersion,[1-3] larger CNNS (about several micrometers) were not in the scope of previous studies. However, the smaller CNNS below 1 μm were difficult to clearly observed by bright field imaging. Here, to get PECL image that was consistent with bright field image, the larger CNNS sample were separated by centrifugation with 8000 r/min for 10 min. The resulting precipitate (larger CNNS sample) was redispersed in ethanol absolute for PECL imaging experiments.

1.3 Photoluminescence characterization of CNNS

The photoluminescence (PL) spectra were performed on a Cary Eclipse, Varian.

1.4 Preparation of electrodes

This part includes the preparation of Si surface, CNNS modification and the electrode fabrication. Most of these methods are similar to our previous work.[4, 5]

Preparation of the Si surface

The *p*-type silicon wafers (1-5 Ω cm resistivity, boron-doped, double side polished, 225-275 μm) (100) and the *n*-type silicon wafers (0.01-0.05 Ω cm resistivity, phosphorus-doped, single side polished, 240-260 μm) (100) were purchased from University Wafers. The wafers were subjected to ultrasonic cleaning for 10 minutes in

sequential baths of acetone, alcohol and ultrapure water. Then dried under an N_2 flow. Then the wafers were cut into 12.5 × 12.5 mm² pieces. Subsequently, the pieces were treated by O_2 plasma with both sides for 30 min. Then pieces were immersed into 5% HF solution for 2 min, washed by ethanol absolute and dried by N_2 flow.

CNNS modification of the Si surface

10 μL CNNS ethanol absolute was immediately dropped onto the surface of freshly prepared Si pieces and dried at room temperature to prepare *p*-Si/CNNS and n^+-Si /CNNS electrode.

Electrode processing

To establish an ohmic contact on the wafer's backside, a corner of the surface was scratched using a diamond glass cutter, ensuring the contact area did not obstruct subsequent LED irradiation. A droplet of InGa eutectic (Sigma Aldrich, 99.99%, metals basis) was applied to the scratched region, followed by the placement of Cu tape. A thin layer of silver paste (Electron Microscopy Sciences) was then applied to cover the InGa eutectic contact and part of the copper tape. After allowing the paste to dry, Kapton tape was used to shield the backside, protecting the ohmic contact.

1.5 Surface characterization

X-ray photoelectron spectroscopy (XPS) measurements were carried out using a VG ESCALAB 250 spectrometer (ThermoFisher Scientific). XPS data processing was performed using the Advantage analysis software. Low resolution scanning electron microscope (SEM) image was performed on a SU7000 (Hitachi) under 20.00 kV with SE mode and magnification 1.38 kx. High resolution SEM image and EDS spectrum was performed on Bruker Nano GmbH Berlin(Germany) under 15.00 kV with SE mode and magnification 12.0 kx. AFM measurements were conducted using a Multimode 8 platform (Veeco, now Bruker) equipped with a silicon tip (ScanAsyst-Air, resonance frequency: 70 kHz, spring constant: 0.4 N/m) in air under Interleave mode.

1.6 Electrochemistry and microscopy experiments

The ECL spectra are recorded continuously with a spectrometer coupled to an optical fiber. The PECL image of CNNS on *p*-Si were recorded with an inverted optical microscope equipped with an EMCCD camera. In these experiments, the

photoelectrodes faced the optical fiber and the objective. Illumination was performed from the backside of the electrode using a light emitting diode (LED, λ_{exc} = 850 nm). In detail, the electrochemical experiments were performed in a 3-electrode cell using a PalmSens4 as a potentiostat. The working electrode was the photocathode with a fixed area of 0.5 cm^2, the reference electrode was an Ag/AgCl (3 M KCl) electrode and the counter electrode was a Pt wire. The Si surface electrode was sealed with an O-ring on the backside of a homemade cell. A transparent glass window on the frontside allowed for the transmission of photons. The electrolyte was composed of 0.1 M $K_2S_2O_8$ dissolved in 0.1 M PBS at pH 7.40. The Si electrode was illuminated from the backside by 850 nm LED (Thorlabs M850L3). The PECL emitted from the Si electrode was transmitted through a shortpass filter with a cut-off wavelength at 750 nm (Thorlabs, FESH0750) in order to remove the IR component from the incident light and was imaged with a horizontal microscope OLYMPUS connected to an EMCCD camera (Hamamatsu). A 40x Objective (APO, NA = 0.8, water objective) were used for images. The exposure time was 15 s for PECL images.

1.7 Image processing

The images in this study were processed using ImageJ software (version 1.54f, National Institutes of Health, Bethesda, MD, USA). The processing steps included brightness and contrast adjustments to optimize image visibility, rotation and cropping to align and extract regions of interest, and color modifications to enhance the visualization of target structures. The panels c in Figure 3 and Figure S7 are coded with the same PECL intensity color scales.

2 Supporting Figures

2.1 LSV of *p*-Si/CNNS

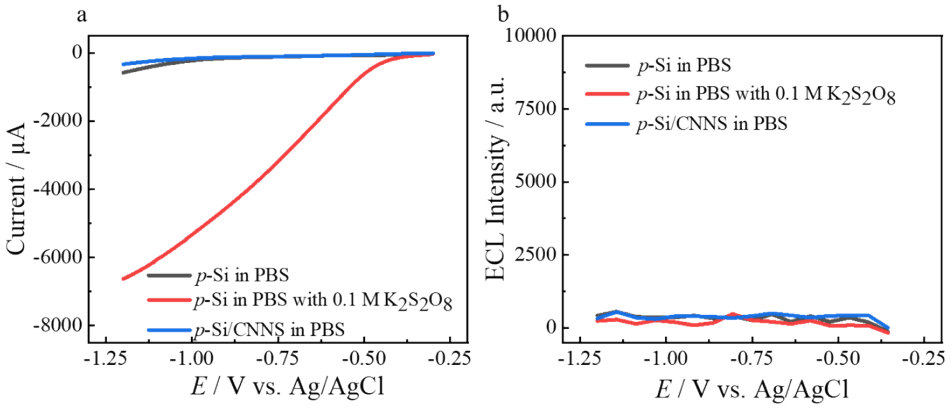

Figure S1 a) LSV recorded on *p*-Si in 0.1 M PBS (black curve), on *p*-Si in 0.1 M PBS containing 0.1 M $K_2S_2O_8$ (red curve), and on the *p*-Si/CNNS photocathode (blue curve) in 0.1 M PBS under IR irradiation. b) Corresponding ECL intensity profiles. Scan rate: 50 mV/s.

The anodic shift in the PECL onset potential arises from the photovoltage generated in the semiconductor under illumination: photogenerated electrons possess sufficient energy to directly reduce $S_2O_8^{2-}$ to $SO_4^{\bullet-}$, thereby reducing the external bias required to drive the reaction. As the applied cathodic bias is progressively increased (i.e., made more negative), band bending at the electrode/electrolyte interface intensifies, strengthening the interfacial electric field. This field effectively suppresses recombination of photogenerated electron–hole pairs and enhances both charge separation and electron injection into the electrolyte. Concurrently, the direct electroreduction of $S_2O_8^{2-}$ at the electrode surface is augmented, collectively boosting the flux of $SO_4^{\bullet-}$ radicals. Consequently, the ECL intensity increases monotonically with increasingly negative bias.

2.2 Emission spectra of n^+-Si/CNNS

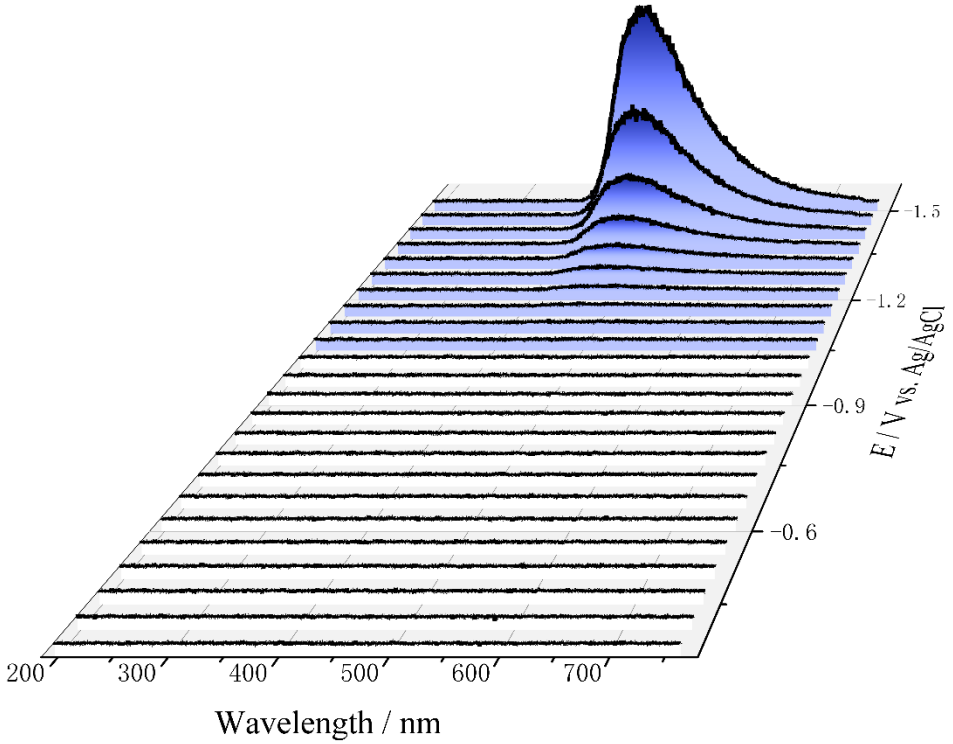

Figure S2 Emission spectra recorded from -0.3 to -1.5 V recorded in the dark on n^+-Si/CNNS. The measurements were performed in 0.1 M PBS with 0.1 M $K_2S_2O_8$. Scan rate: 50 mV/s.

2.3 XPS spectra of *p*-Si/CNNS

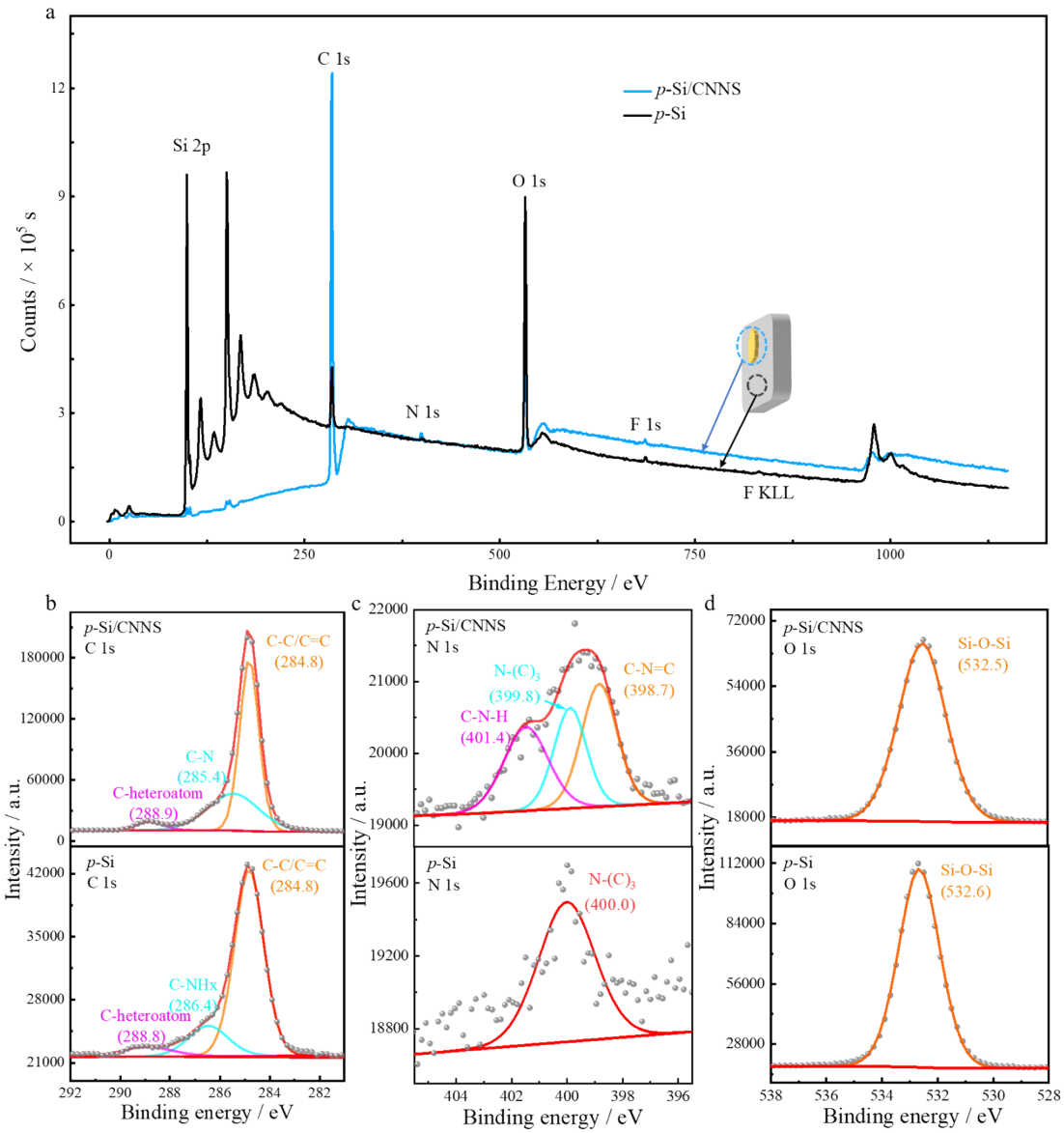

Figure S3 a) XPS of *p*-Si (black) and *p*-Si/CNNS (cyan). b-d) High-resolution XPS spectra of *p*-Si/CNNS. XPS peak of C1s on *p*-Si/CNNS (b, up) and *p*-Si (b, down), N 1s of *p*-Si/CNNS (c, up) and *p*-Si (c, down) and O1s of *p*-Si/CNNS (d, up) and *p*-Si (d, down).

The high resolution XPS spectra of C1s peak and N1s peak[6, 7] was shown in Figure S2 b and c. The C1s spectra (Figure S2, b) revealed the existence of 284.8 eV (sp^2-bonded carbon in C-C/C=C)[1], 285.4 eV (sp^2-bonded carbon in C-N)[6, 7] and 288.9 eV (C-heteroatom)[6, 7]. The N1s spectra (Figure S2, c)[1, 8, 9] revealed the existence of 398.7 eV (sp^2 bonded nitrogen in N-containing aromatic rings (C−N=C)), 399.8 eV(tertiary nitrogen N-$(C)_3$ groups) and 401.4 eV (amino group (C−N−H)). High-resolution XPS spectra of O1s peak was shown in Figure S2, d. The O 1s peak localized at 532.5 eV, originates from the native oxide/hydroxide phase at the underlying SiO_x layer.

2.4 AFM and SEM

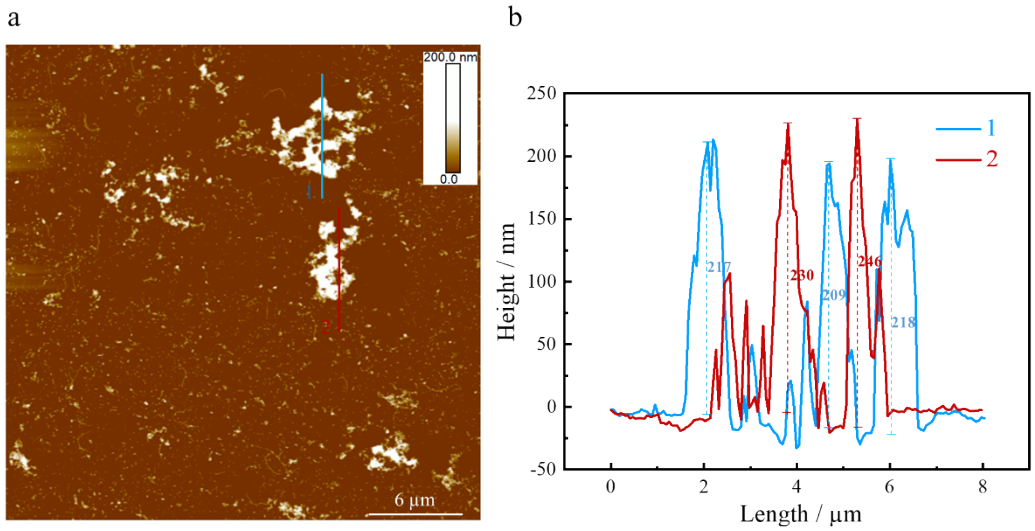

Figure S4 a) AFM image of *p*-Si/CNNS. b) Height profiles of single CNNS extracted from the AFM pictures (a).

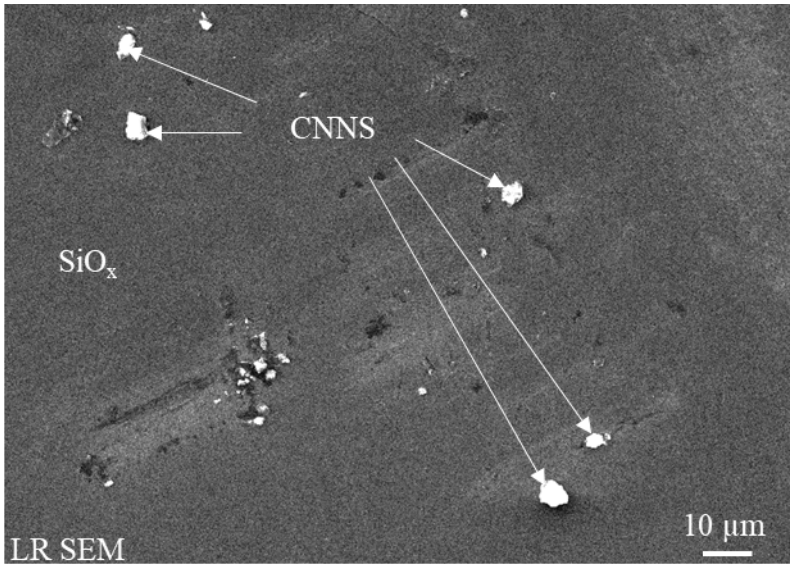

Figure S5 Low-resolution SEM images of CNNS deposited on *p*-Si.

2.5 EDS spectra

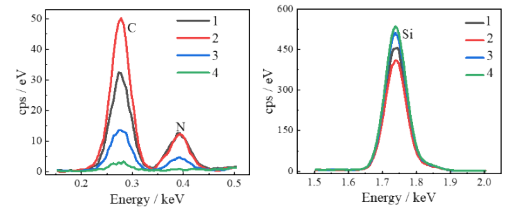

Element	Atomic Number	1 Atom %	2 Atom %	3 Atom %	4 Atom %
C	6	49.64	57.53	43.70	18.85
N	7	22.09	20.23	10.33	/
Si	14	28.26	22.23	45.97	81.15

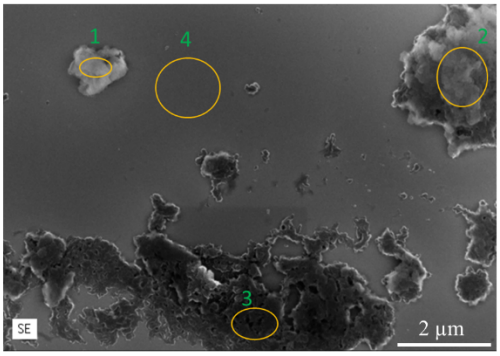

Figure S6 EDS spectra of high-resolution SEM image of *p*-Si/CNNS. EDS spectra (left, up) of C, N and Si marked 1, 2, 3 and 4 in the SEM image(right). Corresponding elemental analysis table of C, N and Si (left, down).

The high-resolution SEM image of *p*-Si/CNNS sample was shown in Figure S5, right. Three CNNS particles and bare Si circled with 1, 2, 3 and 4 in Figure S5, right was chosen to do EDS spectrum analysis of C, N and Si element. There were obvious C, N and Si peaks for CNNS particle circled with 1, 2 and 3 and very weak C peak and strong Si peak for bare Si circled with 4 on their EDS spectrum (Figure S5, left, up). The atom% results of 1, 2 and 3 (Figure S5, left, down) showed the C/N ratio was 2.25:1, 2.84:1 and 4.23:1, respectively. It is not our expected C/N ratio with 3:4 that was prepared by thermal polymerization of dicyandiamide at 500°C for 4 h in air[1]. According to the different proportions of C and N atoms in the framework, a series of C_xN_y materials have been successfully synthesized[10]. The as-reported C_xN_y could be generally classified into two main categories with three- or six-bond-extending frameworks[11]. The diversity of repeating units and bridging groups determines the exact C/N ratios of each different CN, such as C_2N,[7, 12] C_3N,[6] C_3N_2,[13] C_3N_3,[14] C_3N_4,[15] C_4N_3,[16] C_3N_5,[17, 18] C_5N_2,[19] C_4N,[20] C_5N[21] and C_6N_6.[22] These C_xN_y materials can even be converted to each other under certain conditions[11]. Thus, our CNNS should be a mixture of C_2N, C_3N, C_4N and C_5N.

2.6 Current-time plots

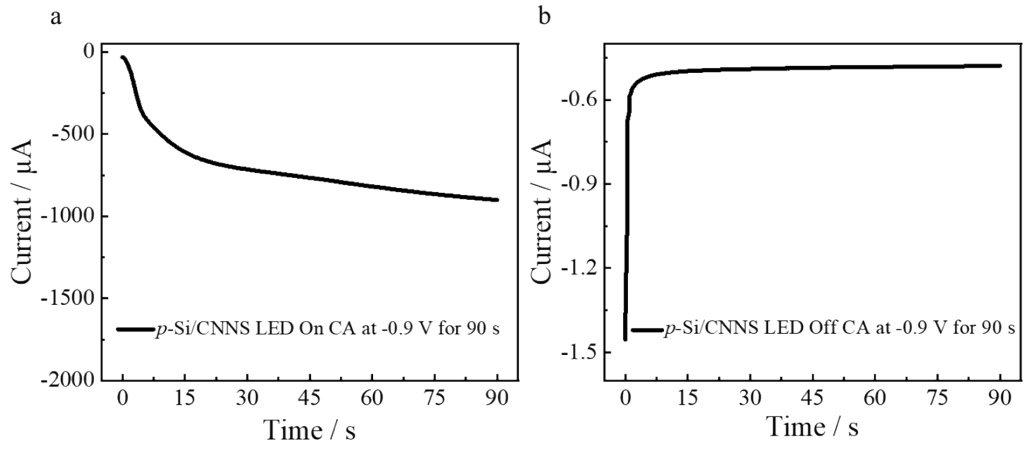

Figure S7 Current-time plots under IR irradiation (a) and in the dark (b) of PECL image recorded on *p*-Si/CNNS at constant potential -0.9 V for 90 s.

2.7 PECL images

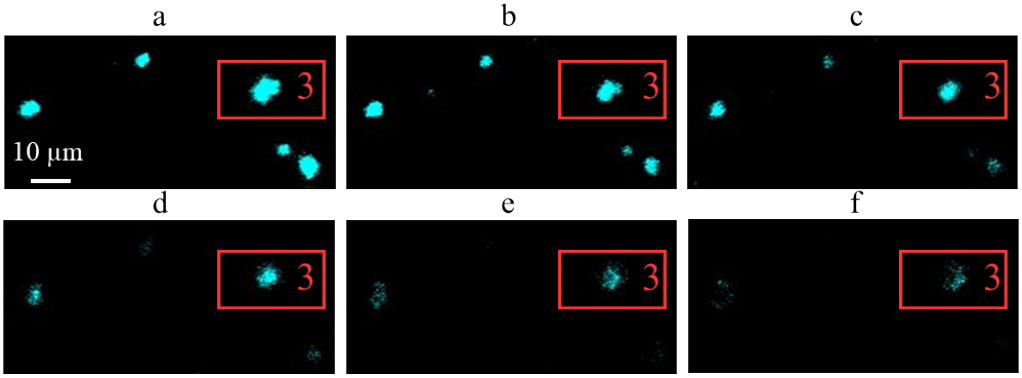

Figure S8 a-f) PECL images of *p*-Si/CNNS under near IR illumination (λ_{exc} = 850 nm) at a constant potential -0.9 V at different time(a) 15 s, (b) 30 s, (c) 45 s, (d) 60 s, (e) 75 s, (f) 90 s.

The ECL images of the CNNS could be affected by i) the exposure time of the EMCCD and ii) the short lifetime of the radicals $SO_4^{\bullet-}$:

i) On one hand, the exposure time of the EMCCD was 15 s. Considering a diffusion coefficient D of $SO_4^{\bullet-}$ (~ 10^{-9} $m^2 \cdot s^{-1}$),[23] the radicals could diffuse over~170 µm using the relation $x \approx \sqrt{2Dt}$. This value greatly exceeds the size of the CNNS (~5 µm).

ii) On the other hand, $SO_4^{\bullet-}$ is a radical with a short lifetime (a half-life of 30–40 µs).[24-26] Considering this value, it implies that it can diffuse up to 3 µm away from electrode surface and this could be a limiting factor to image microscopic objects using $K_2S_2O_8$ coreactant. However, the emitted PECL light is stronger in the centre than at the edges of the CNNS. Therefore, it should not be a limiting factor in the present case.

The time-dependent decay in luminous intensity primarily arises from progressive degradation of the photoelectrode material. Specifically, the *p*-Si substrate is susceptible to photocorrosion under simultaneous illumination and applied bias in aqueous electrolyte, resulting in surface deterioration and impaired charge transfer. Concurrently, the CNNS luminescent component undergoes electrode passivation during prolonged operation: reaction products or intermediates accumulate on its surface, forming a passivating barrier layer that impedes sustained electron transfer and luminescence.

References

1. Ji, J.; Wen, J.; Shen, Y.; Lv, Y.; Chen, Y.; Liu, S.; Ma, H.; Zhang, Y., Simultaneous Noncovalent Modification and Exfoliation of 2D Carbon Nitride for Enhanced Electrochemiluminescent Biosensing. *J. Am. Chem. Soc.* **2017,** *139* (34), 11698-11701.
2. Zhang, Q.; Liu, Y.; Nie, Y.; Liu, Y.; Ma, Q., Wavelength-Dependent Surface Plasmon Coupling Electrochemiluminescence Biosensor Based on Sulfur-Doped Carbon Nitride Quantum Dots for K-RAS Gene Detection. *Anal. Chem.* **2019,** *91* (21), 13780-13786.
3. Zhao, C.; Ma, C.; Jia, S.; Wang, M.; Jiang, M.; Ma, J.; Yu, H.; Hong, C., Ultrathin-N_2C-Deficient Carbon Nitride for Stabilized Enhancement of Electrochemiluminescence. *Small* **2024,** *20* (49), 2403138.
4. Zhou, C.; Descamps, J.; Goudeau, B.; Garrigue, P.; Bedu, F.; Santinacci, L.; Wang, Z.; Sojic, N.; Loget, G., Photoelectrochemical Charge Transfer Imaging at Nanoscale Catalysts. *ACS Energy Lett.* **2025,** *10* (7), 3519-3525.
5. Descamps, J.; Zhao, Y.; Yu, J.; Xu, G.; Léger, Y.; Loget, G.; Sojic, N., Anti-Stokes photoinduced electrochemiluminescence at a photocathode. *Chem. Commun.* **2022,** *58* (47), 6686-6688.
6. Mahmood, J.; Lee, E. K.; Jung, M.; Shin, D.; Choi, H. J.; Seo, J. M.; Jung, S. M.; Kim, D.; Li, F.; Lah, M. S.; Park, N.; Shin, H. J.; Oh, J. H.; Baek, J. B., Two-dimensional polyaniline (C_3N) from carbonized organic single crystals in solid state. *Proc. Natl. Acad. Sci. U.S.A.* **2016,** *113* (27), 7414-7419.
7. Mahmood, J.; Lee, E. K.; Jung, M.; Shin, D.; Jeon, I. Y.; Jung, S. M.; Choi, H. J.; Seo, J. M.; Bae, S. Y.; Sohn, S. D.; Park, N.; Oh, J. H.; Shin, H. J.; Baek, J. B., Nitrogenated holey two-dimensional structures. *Nat. Commun.* **2015,** *6* (1), 6486.
8. Huang, C.; Wen, Y.; Ma, J.; Dong, D.; Shen, Y.; Liu, S.; Ma, H.; Zhang, Y., Unraveling fundamental active units in carbon nitride for photocatalytic oxidation reactions. *Nat. Commun.* **2021,** *12* (1), 320.
9. Fang, Y.; Yang, H.; Hou, Y.; Li, W.; Shen, Y.; Liu, S.; Zhang, Y., Timescale correlation of shallow trap states increases electrochemiluminescence efficiency in carbon nitrides. *Nat. Commun.* **2024,** *15* (1), 3597.
10. Zhang, H.; Zhang, J.; Chen, W.; Tao, M.; Meng, X.; Zhang, Y.; Zuo, G., Insight into structure evolution of carbon nitrides and its energy conversion as luminescence. *Carbon Energy* **2024,** *6* (2), e463.
11. Yang, H.; Wang, Z.; Liu, S.; Shen, Y.; Zhang, Y., Molecular engineering of C_xN_y: Topologies, electronic structures and multidisciplinary applications. *Chin. Chem. Lett.* **2020,** *31* (12), 3047-3054.
12. Tian, Z.; López-Salas, N.; Liu, C.; Liu, T.; Antonietti, M., C_2N: A Class of Covalent Frameworks with Unique Properties. *Adv. Sci.* **2020,** *7* (24), 2001767.
13. Yang, H.; Zhou, Q.; Fang, Z.; Li, W.; Zheng, Y.; Ma, J.; Wang, Z.; Zhao, L.; Liu, S.; Shen, Y.; Zhang, Y., Carbon nitride of five-membered rings with low optical bandgap for photoelectrochemical biosensing. *Chem* **2021,** *7* (10), 2708-2721.
14. Feng, J.; Li, M., Large-Scale Synthesis of a New Polymeric Carbon Nitride—C_3N_3 with Good Photoelectrochemical Performance. *Adv. Funct. Mater.* **2020,** *30* (23), 2001502.
15. Jürgens, B.; Irran, E.; Senker, J.; Kroll, P.; Müller, H.; Schnick, W., Melem (2,5,8-Triamino-tri-s-triazine), an Important Intermediate during Condensation of Melamine Rings to Graphitic Carbon Nitride: Synthesis, Structure Determination by X-ray Powder Diffractometry, Solid-State NMR, and

Theoretical Studies. *J. Am. Chem. Soc.* **2003,** *125* (34), 10288-10300.

16. Zhou, G.; Shan, Y.; Hu, Y.; Xu, X.; Long, L.; Zhang, J.; Dai, J.; Guo, J.; Shen, J.; Li, S.; Liu, L.; Wu, X., Half-metallic carbon nitride nanosheets with micro grid mode resonance structure for efficient photocatalytic hydrogen evolution. *Nat. Commun.* **2018,** *9* (1), 3366.

17. Kim, I. Y.; Kim, S.; Jin, X.; Premkumar, S.; Chandra, G.; Lee, N.-S.; Mane, G. P.; Hwang, S.-J.; Umapathy, S.; Vinu, A., Ordered Mesoporous C_3N_5 with a Combined Triazole and Triazine Framework and Its Graphene Hybrids for the Oxygen Reduction Reaction (ORR). *Angew. Chem. Int. Ed.* **2018,** *57* (52), 17135-17140.

18. Kumar, P.; Vahidzadeh, E.; Thakur, U. K.; Kar, P.; Alam, K. M.; Goswami, A.; Mahdi, N.; Cui, K.; Bernard, G. M.; Michaelis, V. K.; Shankar, K., C_3N_5: A Low Bandgap Semiconductor Containing an Azo-Linked Carbon Nitride Framework for Photocatalytic, Photovoltaic and Adsorbent Applications. *J. Am. Chem. Soc.* **2019,** *141* (13), 5415-5436.

19. Ma, J.; Peng, X.; Zhou, Z.; Yang, H.; Wu, K.; Fang, Z.; Han, D.; Fang, Y.; Liu, S.; Shen, Y.; Zhang, Y., Extended Conjugation Tuning Carbon Nitride for Non-sacrificial H_2O_2 Photosynthesis and Hypoxic Tumor Therapy. *Angew. Chem. Int. Ed.* **2022,** *61* (43), e202210856.

20. Ahmad, I.; Li, F.; Kim, C.; Seo, J.-M.; Kim, G.; Mahmood, J.; Jeong, H. Y.; Baek, J.-B., Robust fused aromatic pyrazine-based two-dimensional network for stably cocooning iron nanoparticles as an oxygen reduction electrocatalyst. *Nano Energy* **2019,** *56*, 581-587.

21. Mahmood, J.; Lee, E. K.; Noh, H.-J.; Ahmad, I.; Seo, J.-M.; Im, Y.-K.; Jeon, J.-P.; Kim, S.-J.; Oh, J. H.; Baek, J.-B., Fused Aromatic Network with Exceptionally High Carrier Mobility. *Adv. Mater.* **2021,** *33* (9), 2004707.

22. Hong, Q.; Yang, H.; Fang, Y.; Li, W.; Zhu, C.; Wang, Z.; Liang, S.; Cao, X.; Zhou, Z.; Shen, Y.; Liu, S.; Zhang, Y., Adaptable graphitic C_6N_6-based copper single-atom catalyst for intelligent biosensing. *Nat. Commun.* **2023**, *14* (1), 2780.

23. Janusz, J. N.; Beeler, J. A.; Hosseini, S.; Tanwar, M.; Zeng, R.; Wang, H.; Abruña, H. D.; Neurock, M.; White, H. S., The Electrochemical Peroxydisulfate-Oxalate Autocatalytic Reaction. *J. Am. Chem. Soc.* **2024**, 146(36), 25088-25100.

24. Zhou, P.; Fu, W.; Ding, L.; Yan, Y.; Guo, W.; Su, B., Toward mechanistic understanding of electrochemiluminescence generation by tris (2, 2′-bipyridyl) ruthenium (II) and peroxydisulfate. *Electrochim. Acta* **2023**, *439*, 141716.

25. Wang, W.; Chen, M.; Wang, D.; Yan, M.; Liu, Z., Different activation methods in sulfate radical-based oxidation for organic pollutants degradation: Catalytic mechanism and toxicity assessment of degradation intermediates. *Sci. Total Environ.* **2021**, *772*, 145522.

26. Shiraz, A. D.; Takdastan, A.; Borghei, S. M., Photo-Fenton like degradation of catechol using persulfate activated by UV and ferrous ions: Influencing operational parameters and feasibility studies. *J. Mol. Liq.* **2018**, *249*, 463-469.